ELSEVIER

Earth and Planetary Science Letters 197 (2002) 133–149

EPSL

www.elsevier.com/locate/epsl

Deep structure and mechanical behavior of the lithosphere in the Hangai–Hövsgöl region, Mongolia: new constraints from gravity modeling

Carole Petit [a,*], Jacques Déverchère [b], Eric Calais [e], Vladimir San'kov [c], Derek Fairhead [d]

[a] *Laboratoire de Tectonique, ESA 7072, T 26 E 1, Boîte 129, 4 place Jussieu, 75252 Paris Cedex, France*
[b] *UMR 6526 Géosciences Azur, CNRS-UPMC-UNSA-IRD, P.O. Box 48, 06235 Villefranche sur Mer Cedex, France*
[c] *Institute of the Earth's Crust, SB RAS, Irkutsk, Russia*
[d] *GETECH, c/o School of Earth Sciences, University of Leeds, Leeds LS2 9JT, UK*
[e] *Dept. of Earth and Atmospheric Sciences, Purdue University, West Lafayette, IN 47907-1397, USA*

Received 26 June 2001; received in revised form 31 December 2001; accepted 8 January 2002

Abstract

We investigate the deep structure and mechanical behavior of the lithosphere beneath the Hangai–Hövsgöl region, central Mongolia, Asia, in order to explain the origin and support of large-scale doming in this deforming area. We propose a gravity- and topography-based model which accounts for constraints provided by other independent results from xenolith and tomography studies. Deviations of the measured gravity from the theoretical Airy-compensation model are examined. A long-wavelength low-gravity anomaly is spatially correlated with low pressure and shear velocity anomalies in the mantle, and with the extent of Cenozoic volcanic outcrops. We interpret it as a deep-seated low-density asthenosphere and model its effect on the Bouguer gravity signal using a 600 km wide light asthenospheric body (density reduction -10 kg m^{-3}) located between 100 and 200 km. North and south of the Hangai–Hövsgöl dome, short-wavelength highs and lows in the Bouguer gravity field are clearly correlated with fault activity. They seem to reflect opposite senses of flexure of a rigid lithosphere across two major active faults, the Sayan and Bogd transpressional systems, and are modeled by Moho deflections of 10 and 5 km, respectively. Finally, a short-wavelength (200 km), high-amplitude (-50 mGal) gravity residual remains beneath the highest part of the mountain bulge, namely the Hangai dome. Based on previously published xenolith analyses, we interpret it as an anomalous, low-density body which may represent underplated cumulates or mafic granulites at the uppermost mantle. We conclude that upper mantle dynamics necessarily play an important role in the origin and evolution of the Hangai–Hövsgöl dome, but without requiring significant thinning of the lithosphere. © 2002 Elsevier Science B.V. All rights reserved.

Keywords: topography; gravity methods; Mongolia; Hangay Mountains; upper mantle; flexure

* Corresponding author. Tel.: +33-1-4427-3871; Fax: +33-1-4427-5085.
E-mail addresses: carole.petit@lgs.jussieu.fr (C. Petit), jack@obs-vlfr.fr (J. Déverchère), ecalais@purdue.edu (E. Calais), sankov@crust.irk.ru (V. San'kov), d.fairhead@earth.leeds.ac.uk (D. Fairhead).

0012-821X/02/$ – see front matter © 2002 Elsevier Science B.V. All rights reserved.
PII: S0012-821X(02)00470-3

1. Introduction

The origin of reliefs inside continental domains undergoing compressional strain is generally difficult to assess because it results from several mechanisms whose relative importance varies with time (e.g., [1] and references therein). A first end-member mechanism is crustal or lithospheric shortening, involving folding, simple shear, or pure shear ('boudinage') at a lithospheric scale [2,3]. The other end-member mechanism, buoyancy variations in or beneath the lithosphere, resulting from mantle convection or plate tectonics, may also support the topography at different stages of mountain evolution (e.g., [4,5]). Therefore, elucidating the processes responsible for mountain growth requires at least some knowledge of the crust and mantle structures together.

Mongolia, central Asia, is clearly interesting in this respect because its topography is high, obviously young (less than 30 Myr, e.g., [6] and references therein), and depicts contrasting and yet poorly understood features (Fig. 1A). (1) The Sayan, Altai and Gobi–Altai mountains are long, linear belts which bear obvious genetic links with active strike-slip and reverse faulting (e.g., [7,8]). (2) Several elevated bulges have a dome shape and are not clearly related to recent fault activity. The most prominent one is the Hangai–Hövsgöl dome, which is the largest part of the so-called Mongolian Plateau [9]. It is a 800-km-long N–S topographic bulge extending north of the Gobi–Altai range and characterized by elevations typically exceeding the regional trend of ~1.5 km (Fig. 1a). Only few short normal faults have been found in the central part of Hangai [6], where topography is the highest (culminating at ~4000 m), whereas several large-scale E–W strike-slip and reverse faults were active on both sides of it during the last century [8,10,11] (Fig. 1a). (3) The Hangai–Hövsgöl region is covered by sparse Cenozoic and Quaternary basaltic volcanism covering several hundreds of square kilometers [12]. (4) The current strain regime in this area is probably a combination of E–W extension resulting from the eastward motion of the Amurian–North China block [13,14] and NE–SW shortening due to the India–Asia convergence [15].

From the latter observations, most authors have inferred that the far-field effect of the India–Asia collision is the main factor driving mountain growth in Mongolia ([16,17] and references therein). Using gravity and seismological interpretations, or a comparison of igneous activity with the age of tectonic events in the last 40 Myr, several others have invoked the influence of mantle upwelling beneath eastern Asia, and especially the Baikal rift, North China and Mongolia [18–21].

This study aims to clarify the role of faulting, folding and mantle activity in western–central Mongolia. To achieve this, we perform a pseudo-3D forward gravity modeling analysis constrained by other independent data on deep structures. Using deviations from local isostasy, we search for static, buoyancy sources at lithospheric and asthenospheric levels, and for flexural contributions at a crustal scale. We then discuss the relative importance of buoyancy and tectonic forces on recent topography genesis in this part of central Asia.

→

Fig. 1. (a) Topographic map of Mongolia and Baikal regions. Main topographic features are as follows: AL = Aldan Shield; SC = Siberian craton; Ht = Hentai massif; Hg = Hangai massif; Sa, Al and Go are Sayan, Altai and Gobi–Altai mountains, respectively. Black lines are active faults. The main fault systems (Sayan, Bolnai and Bogd) and lakes (Baikal, Hövsgöl) are indicated. Ellipses are approximate zones of Cenozoic volcanics. Inset shows the map location in Asia. Quadrilateral frame shows the area covered by the geologic map shown on Fig. 2. (b) Residual Bouguer gravity (in mGal) map of the Baikal–Mongolia region, defined as the difference between the measured Bouguer gravity and the Airy-isostasy model. Main active faults are shown. Quadrilateral frame shows the position of the 12 gravity profiles processed in this study. Black dot indicates the place where xenoliths were sampled [24–26].

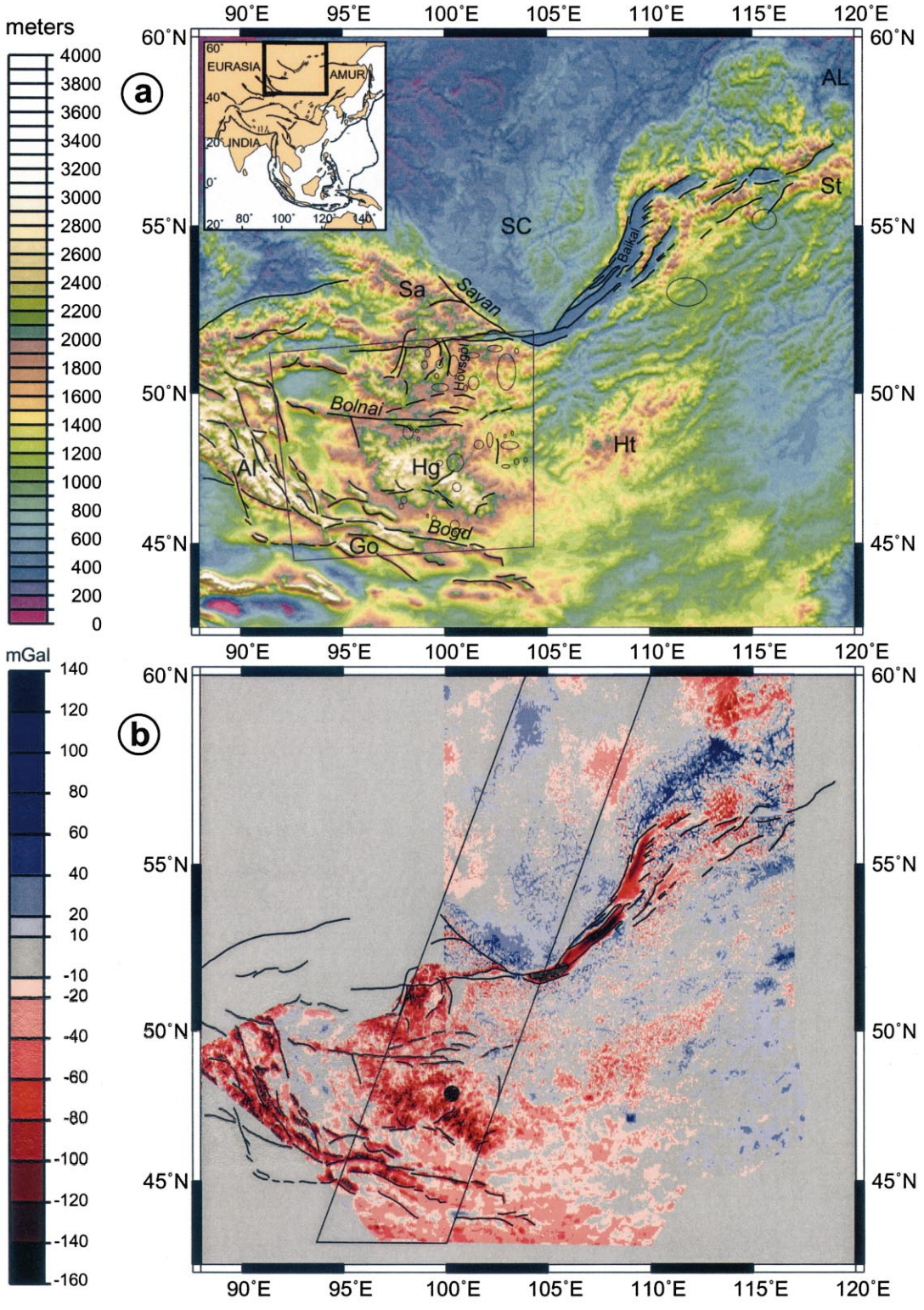
meters
4000
3800
3600
3400
3200
3000
2800
2600
2400
2200
2000
1800
1600
1400
1200
1000
800
600
400
200
0
mGal
140
120
100
80
60
40
20
10
-10
-20
-40
-60
-80
-100
-120
-140
-160
a
b
90°E
95°E
100°E
105°E
110°E
115°E
120°E
60°N
55°N
50°N
45°N
EURASIA
AMUR
INDIA
AL
St
SC
Baikal
Sa
Sayan
Hovsgol
Bolnai
Ht
Al
Hg
Bogd
Go

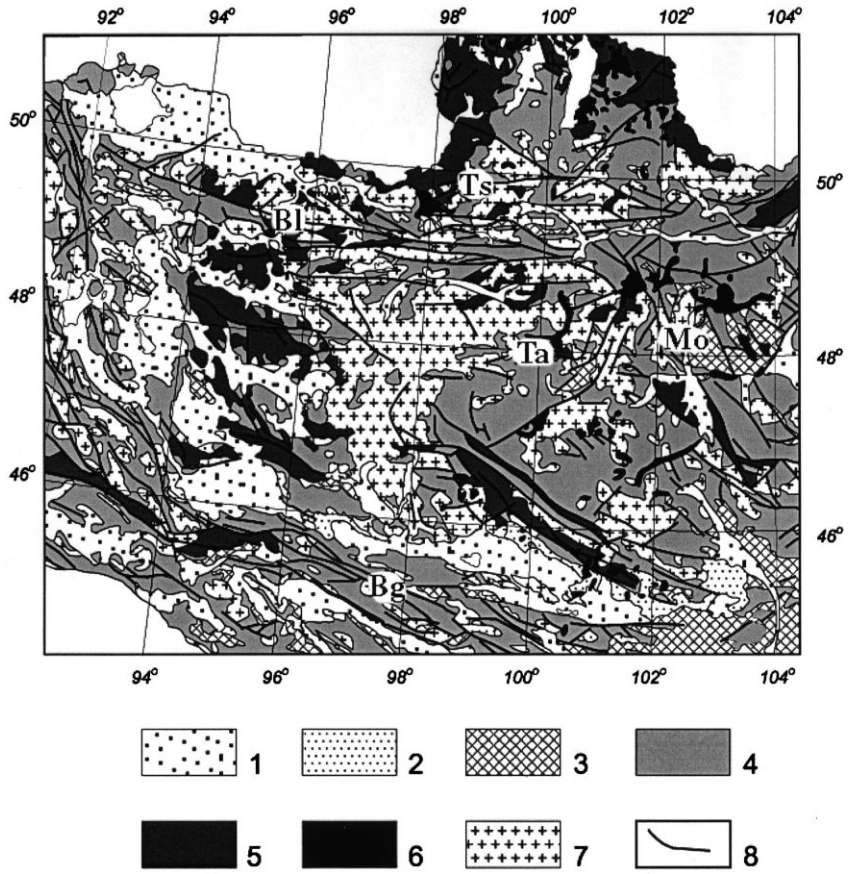

Fig. 2. Geologic map of the Hangai–Hövsgöl upland region and Gobi–Altai (see location in Fig. 1), modified from [22]. (1) Pliocene–Quaternary deposits; (2) Paleogene–Neogene deposits; (3) Mesozoic sedimentary and volcano-sedimentary rocks; (4) Paleozoic sedimentary and volcano-sedimentary rocks; (5) Precambrian metamorphic and igneous rocks (undifferentiated); (6) Cenozoic basalts; (7) Paleozoic–Mesozoic intrusive rocks (undifferentiated); (8) Main faults. Bg = Bogd (Gobi–Altai) fault; Bl = Bolnai fault; Ts = Tsetserleg fault; Mo = Mogod fault; Ta = Tariat volcanic field.

2. Tectonic evolution and lithospheric structures in central Mongolia

2.1. Pre-Cenozoic geology and Cenozoic evolution

A detailed overview of the geodynamic history of the Mongolia–Siberia region is given by Zorin [22]. We recall it briefly and compare it with the main present-day topographic and tectonic features based on previous work summarized by Cunningham [6,17]. The basement of the Hangai dome is an old Precambrian continental block overlain by thick Paleozoic turbidites and intruded by Permian granitoids [23] (Fig. 2). These formations come from the collision between West Mongolia and Siberia in the Early Permian, followed by progressive closure of the Mongol–Okhotsk ocean towards the east during the Jurassic [22]. The Altai and Gobi–Altai belts developed on accreted Paleozoic terranes (subduction/accretion complexes). Surface geology of the Hangai dome is similar to that of surrounding regions, i.e., Paleozoic sediments and volcanics with intrusive granitoids. Recent formations (Cenozoic) consist mainly of basaltic emissions (in black in Fig. 2) and shallow sedimentary basins.

Paleozoic and Mesozoic orogenic episodes have intensely fractured the crust into large faults of

northward vergence in our study region [22], and it seems obvious that present-day deformation preferentially follows inherited structural trends [6,17]. Active tectonic features consist mainly of strike-slip and reverse faults in the Altai and Gobi–Altai, and normal faults bounding Cenozoic basins in the Hövsgöl region (Figs. 1 and 2). Recent volcanism (from ~9 Ma to present [12]) outcrops in several parts of the region, without visible time–space dependence. The timing of Cenozoic mountain building in Mongolia is not accurately constrained [6], but it appears that most of the present-day topography postdates a Paleocene peneplanation surface and is generally assigned an Oligocene to early Miocene age [6,7,10].

2.2. Present-day lithospheric and crustal structures

Unfortunately, crustal-scale seismic data are lacking in Mongolia. The best-constrained structural information comes from thermobarometric and petrologic analyses of young xenoliths in the Tariat region (Hangai) (Fig. 1b and [24–26]) which indicate: (1) an average crustal thickness of 46 km in western Mongolia; (2) a maximum crustal thickness of 50 ± 3 km beneath the northern Hangai area, where pressure equilibration conditions from the shallowest ultramafic rocks range around 1.4×10^3 MPa; (3) evidence for intrusion of asthenospheric material in the lithosphere at depths well below 70 km; (4) a thermal anomaly at the uppermost mantle, as indicated by a high-curvature geotherm around 40–50 km which can reflect heat advection from basaltic intrusions, and by underplated cumulates near the Moho. However, the average heat flow in Mongolia is still moderate (~60 mW $m^{-2)}$ [27]).

Recently, several global and regional seismic tomography models in Asia have consistently imaged a deep-seated (around and below 100 km) low-velocity anomaly beneath central Mongolia (e.g., [28–30]). The new shear-wave velocity model obtained by Villaseñor et al. [31] from inversion of surface wave velocities further strengthens this view: it depicts a large low-velocity anomaly beneath the Hangai–Hövsgöl region at about 100 km depth, with a −4% contour line fitting approximately the broad uplands of Hangai and Hövsgöl, whereas no anomaly is found below Lake Baikal. The surface projection of the Hangai–Hövsgöl shear-wave velocity anomaly correlates quite well with widely spread volcanic emissions dated between Paleogene and Quaternary [12,32], extending over more than 1000 km from north to south across Mongolia on a width of about 600 km [12] (Fig. 2). Although this volcanic activity suggests the presence of a low-density, hot asthenosphere beneath the Hangai–Hövsgöl region, the relatively low regional heat flow [27] with respect to the time duration of volcanic emissions (~9 Ma), the xenolith analyses (see above) and the lack of space–time correlation of volcanic emissions argue against the existence of a very high-heat flux plume (or 'hot-spot') below the Hangai–Hövsgöl dome. Until now, tomographic studies have not accurately constrained the depth extent of this low-velocity body.

3. Gravity models

We use a new dataset, a 8×8 km Bouguer gravity map provided by Geophysical Exploration Technology (GETECH, University of Leeds, UK) covering the Baikal–Mongolia area. Bouguer gravity anomalies are terrain-corrected and are calculated from free-air anomalies using a mean crustal density of 2670 kg m^{-3}. The topography is taken from the GTOPO30 database. We extracted 12 1800-km-long and 10-km-large swaths for our analysis, spaced every ~35 km crossing western Mongolia from the Gobi–Altai range (south) to the Siberian craton (north) and encompassing the Hangai–Hövsgöl dome in its larger width (Fig. 1b).

3.1. Airy model: implications from fits and misfits

We first compute the Bouguer gravity anomaly resulting from a local, Airy-type compensation of the topography. This computation is performed in three dimensions with the GMT software [33] which uses a first-order truncation of the Parker formulation. We use a mean density for the crust and upper mantle of 2670 kg m^{-3} and 3200 kg m^{-3}, respectively. The initial (i.e., zero-topogra-

phy) depth to the Moho is 40 km, as previously determined in the Baikal–Mongolia region from deep seismic soundings [34]. Then we compute a residual gravity anomaly, defined as the difference between the measured Bouguer gravity and the predicted one (Fig. 1b):

$$\Delta g_{\mathrm{Res}} = \Delta g_{\mathrm{Meas}} - \Delta g_{\mathrm{Airy}} \quad (1)$$

Null (zero) residuals means that the topography is locally compensated; positive/negative residuals depict a density excess/deficit. Depending on their wavelength, these residuals can be interpreted as an under-/overcompensation of the topography, compared to the Airy compensation model. Various interpretations can then arise: for instance, a flexural redistribution of stresses must be accounted for, or three-dimensional mass density variations within the lithosphere are responsible for topography/gravity anomalies. In reality, both may occur.

Our aim is thus to determine the possible sources of gravity residuals, depending on their wavelength and on their spatial relationships with tectonic and magmatic features.

3.1.1. Long-wavelength residuals (∼600 km)

A striking feature of the gravity residual map is the existence of large-scale isostatic anomalies in Mongolia (southwest of Fig. 1b). Most of these long-wavelength gravity residuals cannot be explained by recent fault activity. In particular, the Hangai–Hövsgöl region is characterized by a long-wavelength (∼600 km) negative (∼20–30 mGal) residual (Fig. 1b). Several hypotheses arise: (1) crustal density variations: however, the geological history – and probably, the deep crustal structure – of the Hangai–Hövsgöl region is very similar to that of surrounding regions (i.e., Sayan–Baikal) areas, where no gravity residual is found [22]. Hence, we argue that such large-scale crustal density variations are unlikely to be the reason for this long-wavelength residual. In any case, rescaling the measured Bouguer gravity with a lower crustal density would not reduce the residual since we would need to reduce the topography load and compensation effect as well; (2) additional Moho deflection linked to downward buckling of the lithosphere: but maintaining the Moho deeper than predicted by the Airy model over 600 km would require an effective elastic thickness of more than 100 km, and huge bending stresses; (3) mantle contribution: we note that this residual coincides with the deep, low-velocity zone imaged beneath 100 km by teleseismic tomography, and with the spatial extent of Cenozoic volcanism ([12,31]; Fig. 2).

We thus hypothesize that the long-wavelength Bouguer anomaly residual encountered in the Hangai–Hövsgöl region is caused by a low-density asthenosphere located below 100 km, as suggested by its wavelength, by tomographic models, and by xenoliths analyses.

3.1.2. Short-wavelength residuals (100–200 km)

In the Baikal area, most of the short-wavelength (∼100 km), uncompensated topography is located close to the rift faults, advocating the role of tectonic processes in topography genesis [35,36] (Fig. 1b). This is also the case in the Altai and Gobi–Altai ranges (south-west) close to major strike-slip and reverse faults (such as the Bogd fault system, see Fig. 1a). Finally, a strong positive residual is found north of the Sayan fault bounding the Siberian craton, showing that the northern wall of the fault (craton) is undercompensated. We therefore suggest, as proposed by Karner and Watts [37], Burov et al. [35] or Caporali [38], that the Moho is maintained at depths different than predicted by the Airy model across these faults by vertical forces acting on rigid lithospheric plates. These forces are linked to complex tectonic interactions between far-field horizontal compressional forces and active faults; for instance, they can result from focused lower crustal flow in response to compression or to plate loading due to surface thrusting. Although Bogd and Sayan faults depict dominant left-lateral strike-slip components, significant dip-slip motions can occur along favorably oriented parts of them. For instance, previous studies have shown that mountain building occurs along the Bogd fault by the way of numerous restraining bends causing positive flower structures at the surface [8,10,11] that might be compensated by similar crustal thickening at the Moho. A modeling study has shown

that the isostatic residual encountered south of the Sayan fault can be explained by deep crustal thickening in response to far-field compression [36]. Results of two-dimensional forward modeling of lithospheric flexure will be detailed in Section 3.2.

3.2. Static and dynamic forward gravity models

3.2.1. Three-dimensional static model of a low-density asthenosphere

First, we compute the three-dimensional Bouguer anomaly resulting from a low-density body covering approximately the Hangai–Hövsgöl region (500×700 km, Fig. 3), in order to reproduce the effects of a low-density asthenospheric body. Sphericity effects are not taken into account. The lateral extent of the low-density body is chosen according to the most accurate images obtained from regional [30] and surface wave [31] tomography studies. This forward modeling of the gravity source has been performed in parallel with downward continuation of the long-wavelength gravity field to 100 km. The shape of the low-density body is constrained by 12 parallel gravity profiles spaced every 30′ of longitude (i.e., ∼35 km) (Fig. 3). However, given the lack of resolution of tomography results at depth, we have little constraint on the depth extent of this low-density body; the shear-wave velocity model of Villaseñor et al. [31] indicates a 4% velocity reduction at a depth of 100 km. As determined empirically by Deschamps et al. [39], the scaling factor between density and shear velocity variations in the upper mantle abruptly changes beneath 220 km for continental regions, due to complex dependences for temperature and melt generation. Therefore, we have no a priori constraints on density variations beneath 200 km, and we decide to limit our gravity model to this depth. Clearly, there is a trade-off between the density reduction and thickness of the low-density body, which we cannot solve without other constraints. We test density contrasts of −10, −20 and −30 kg m^{-3}. The best-fitting density contrast is small (−10 kg m^{-3}) and corresponds to the volumetric expansion caused by a temperature increase of 100°C, with an initial density of 3200 kg m^{-3}. This value is consistent with geotherms computed from mantle xenolith analyses [24–26]. According to Deschamps et al. [39], the scaling factor relating Vs to ρ is: $\chi = \delta\ln(Vs)/\delta\ln(\rho) \approx 0.05$).

From 100 to 200 km beneath continents, a density variation of 10 kg m^{-3} would correspond to a shear velocity reduction of ∼5%, in agreement with recent tomography studies [31]. Thus, we find that a low-density asthenosphere is a good explanation for the long-wavelength gravity residual found in the Hangai–Hövsgöl region (Fig. 3). Taking this effect into account, it appears now that short-wavelength residuals are particularly clear on the profiles close to the Sayan fault system and on the map around the Bogd fault system. Residuals are of maximum amplitude and opposite senses close to the faults and decrease perpendicular to the fault, suggesting an effect of lithospheric flexure at the vicinity of these faults.

3.2.2. Two-dimensional dynamic model of lithospheric flexure across faults

In order to reproduce the lithospheric flexure near faults, we use the semi-analytical approach developed by Burov et al. [35] and Burov and Diament [40], who model the vertical deflection of a lithosphere caused by distributed loads (topography) and horizontal and vertical tectonic forces. This approach is two-dimensional, hence we present here the modeling results for the 12 closely spaced profiles, which provides a pseudo-3D view of the lithospheric flexure. The modeling approach is explained in detail by Burov et al. [35] and Burov and Diament [40] and we merely recall here its main aspects. Brittle–elasto-ductile plate rheology is constrained by laboratory measurements extrapolated to geological time frames [41], geothermal gradients [12,27,33], crustal and lithospheric thicknesses inferred from gravity anomalies [18,36], and crustal composition deduced from petrology and seismology [19,24–26,33,42]. In these rheological models, ductile behavior of the lower crust and lower lithosphere is represented by power law creep:

$$\dot{\varepsilon} = A^* \exp(H^*/RT)(\sigma_1 - \sigma_3)^n \quad (2)$$

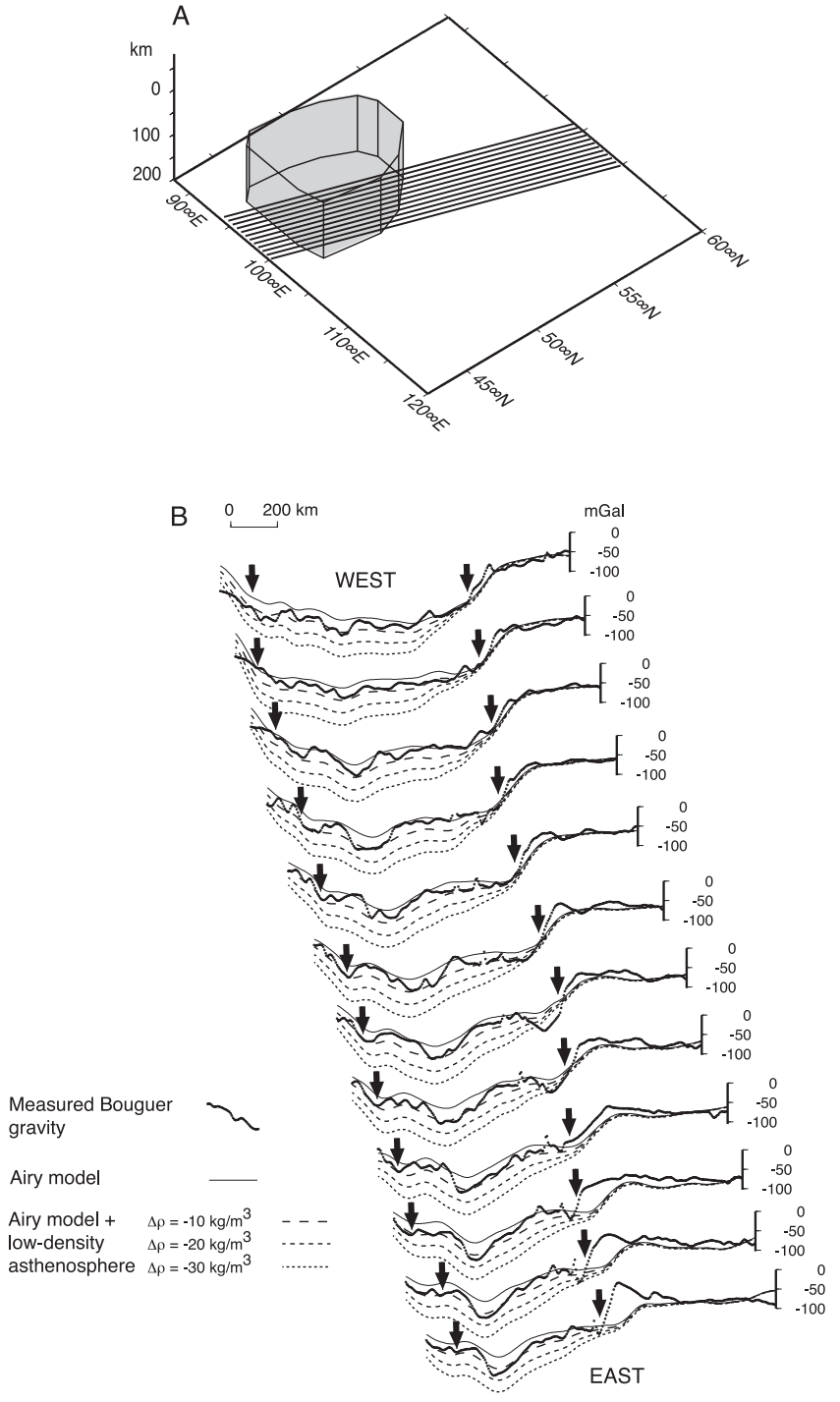

Fig. 3. (A) Geometry of a low-density body (inset) located between 100 and 200 km, with variable density reductions. Lateral extent of the body is approximately 600 km. The 12 parallel lines correspond to the profiles shown below. (B) Twelve gravity profiles spaced from west (top) to east (bottom) across the Hangai–Hövsgöl region, showing the effect of the low-density asthenosphere added to a local, Airy-type compensation model. Spacing between lines is about 35 km. See Fig. 1b for location. Solid arrows indicate the location of Bogd (south) and Sayan (north) faults.

with A^* is the power law stress constant, H^* is the activation energy and n is the power law exponent ($A^* = 6.31 \times 10^{-20}$ Pa^{-n} s^{-1} and $A^* = 7.0 \times 10^{-14}$ Pa^{-n} s^{-1} for diabase and olivine, respectively; H^* is the activation enthalpy with $H^* = 276$ kJ mol^{-1} and 520 kJ mol^{-1} for diabase and olivine, respectively; R is the gas constant; T is the absolute temperature at the given depth; and n is the power law exponent ($n = 3.05$ and 3 for diabase and olivine, respectively).

Brittle failure in the upper crust and upper mantle is controlled by the Von Mises criterion [43]:

$$\sigma_2 = (\sigma_1 - \sigma_3)/3.9,\ \sigma_3 < 120 \text{ MPa}$$
$$\sigma_2 = (\sigma_1 - \sigma_3)/2.1 - 100,\ \sigma_3 \geq 120 \text{ MPa} \quad (3)$$

The elastic parts are modeled assuming Young's modulus E of 1 GPa and Poisson's ratio ν of 0.25. During loading, deflection of the lithosphere is computed as the one of an elastic plate with space-variable T_e. The effective elastic thickness of plate is estimated through a nonlinear function $\tilde{T}_e = \tilde{T}_e(\Phi)$ such as:

$$\tilde{T}_e^3 = \frac{\tilde{D}(\Phi)}{D_0} = \frac{-\tilde{M}_x(\Phi) R_{xy}}{D_0} = \frac{\tilde{M}_x(\Phi)}{D_0} \left(\frac{\partial w(x)^2}{\partial x^2} \right)^{-1} \quad (4)$$

Where $D_0 = E[12(1-\nu^2)]^{-1}$ is the initial rigidity, $R_{xy} \approx -(w'')^{-1}$ is the radius of plate curvature, $w(x)$ is the vertical deflection of the plate, and $\tilde{M}_x$ is the bending moment.

It is important to note that plate bending may lead to inelastic (brittle or ductile) deformation where bending stresses exceed the yielding limits. The nonlinear feedback between local strength and plate structure is solved by an iterative numerical approach (see [40] for details).

Plate discontinuities can be introduced in the model, as free-slip vertical bands delimiting semi-infinite plates. They do not represent the frictional behavior of true faults, which is very different from free-slip, but major weakness zones where flexure is likely to occur. Vertical forces are applied on both sides of plate discontinuities in order to reproduce the plate flexure. Vertical forces account for tectonically induced vertical stresses such as fault-related bending (thrusting) and/or focused lower crustal flow, combined with frictional behavior of faults.

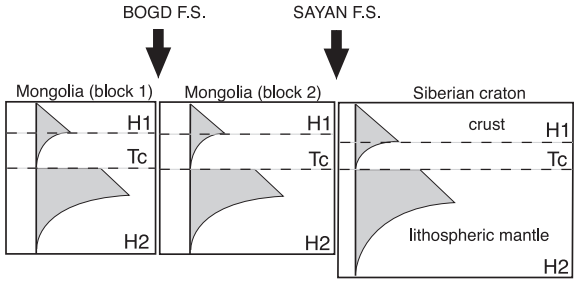

Fig. 4. Initial rheological layering used for forward modeling of the plate flexure (see text for details); initial parameters H1, H2 and Tc are indicated. We use three lithospheric plates separated by two discontinuities corresponding to the Sayan and Bogd Fault systems (see Figs. 1A and 2 for fault location).

The plate rheology is described by three parameters [39] (Fig. 4): H1 (depth of brittle/ductile transition in the crust), Tc (Moho depth) and H2 (bottom of mechanical lithosphere). Their initial values were chosen in order to fit the lithospheric structure and thermal age previously discussed: Tc is 40 km [36], H2 is 80 km for the Mongolian region and 120 km for the Siberian craton [18,36], and H1 is 20 km in Mongolia and 25 km in the Siberian craton [42] (Fig. 4). These values correspond to a diabase (crust)–olivine (mantle) composition, with thermal ages of 100 and 200 Ma for the Mongolian area (very similar to the crustal rheology inferred from depth distribution of earthquakes in the Baikal rift by Déverchère et al. [42]) and the cratonic area, respectively. No horizontal boundary forces are applied since we model only the vertical forces coming from the local dip-slip component of movement on major faults that are locally responsible for plate flexure. We introduce two discontinuities representing the Bogd and Sayan faults (Fig. 1), with opposite flexures across these faults. The Bolnai fault is not detectable on the Bouguer gravity, thus we consider that there is no significant vertical motion on this fault at a crustal scale. Many tests have been performed on each profile to constrain the best-fitting plate deflection (in the sense of minimum root mean square resid-

ual) with respect to the measured gravity signal. The gravity signature of the low-density asthenosphere described above is added to the output gravity model. The best-fitting model implies a step in the Moho of ~5 km for the Bogd fault and ~10 km for the Sayan fault (Fig. 5), the northern wall being uplifted and the southern wall being downpulled. The Moho offset is due to downward bending of the uppermost mantle; hence, it implies that the uppermost mantle can retain significant elastic strength, otherwise the offset would be rapidly diffused by ductile flow. The brittle parts of the lithosphere are much stronger under compression than extension; given our initial rheology (the mantle elastic thickness is about 20 km, see Fig. 4), bending stresses due to high plate curvature close to the fault would not be high enough to induce a ductile behavior at the uppermost mantle (e.g., [36,40]). It therefore appears that plate flexure is able to explain short-wavelength gravity residuals near large faults. Compared to the Airy model, the flexural model allows a better explanation of the amplitude of the short-wavelength (100–200 km) gravity signal, except over the highest part of the Hangai dome where a strong (40–50 mGal) negative residual is still observed, especially in the easternmost profiles.

3.2.3. *Remaining gravity residual of the Hangai dome: an uppermost mantle anomaly?*

The wavelength (~200 km) and amplitude (~50 mGal) of the major remaining gravity residual suggest that the source of this anomaly is located not much deeper than the Moho. Crustal overthickening, possibly due to pure-shear shortening of the crust, could be an explanation for this residual. However, one must note that the maximum Moho depth predicted by the Airy compensation model is 55 km (with an initial crustal thickness of 40 km), not enough to explain the measured ~−300 mGal gravity anomaly. Matching the measured Bouguer gravity over the Hangai dome by crustal overthickening (i.e., considering a crustal root deeper that predicted by the Airy model) would require a ~60-km-deep Moho, a value which is higher than the maximum of 53 km expected from the lowest-temperature lherzolite [24–26]. Moreover, one should question the origin of this assumed crustal thickening. Indeed, it cannot result from upper crustal overthrusting since: (1) there are no major thrusts where crustal thickening could occur; and (2) thickening of the upper crust cannot explain the presence of a deep (i.e., deeper than the Airy model prediction) crustal root. Hence, crustal thickening, if existing, should only result from lower crustal flow converging beneath the Hangai massif, possibly in response to downward buckling of the upper mantle. Numerical mechanical modeling could show whether such a large crustal flow – necessary for creating surface topography associated with downward buckling of the Moho – is possible or not. Nevertheless, taking into account the maximum depth of 53 km postulated for the Moho, this explanation is still unlikely.

We have therefore to advocate another cause, the presence of an anomalous, low-density uppermost mantle or lower crust. Based on evidence from thermal perturbations at the uppermost mantle described by Ionov et al. [26], we propose that a low-density body at the Moho (i.e., in the lower crust and/or uppermost mantle) can be the source of gravity anomalies. Uppermost mantle xenoliths have shown occurrences of mafic granulites within the uppermost mantle – whose depth is defined by the lowest-temperature lherzolite [24] – and of underplated pyroxenites [25,26]. The high density reduction is in better agreement with the presence of intrusive mafic granulites in the uppermost mantle, rather than underplated pyroxenites which are only slightly (40–50 kg m^{-3}) lighter than surrounding lherzolites (see Section 4) [44].

Using the same forward modeling procedure as for the deep-seated density anomaly, we test density contrasts of −200, −250 and −300 kg m^{-3} for a prism 10 km thick, 400 km long and 100 km wide located just beneath the Moho (Fig. 6). Since 10 km appears as a maximum thickness (see Section 4) we did not test density reductions of less than 200 kg m^{-3}. We find that a density reduction of 200 kg m^{-3} fits well the observed gravity residual of −50 mGal. A thinner/thicker prism with a higher/lower density reduction would produce the same effect, but we have no means to solve this

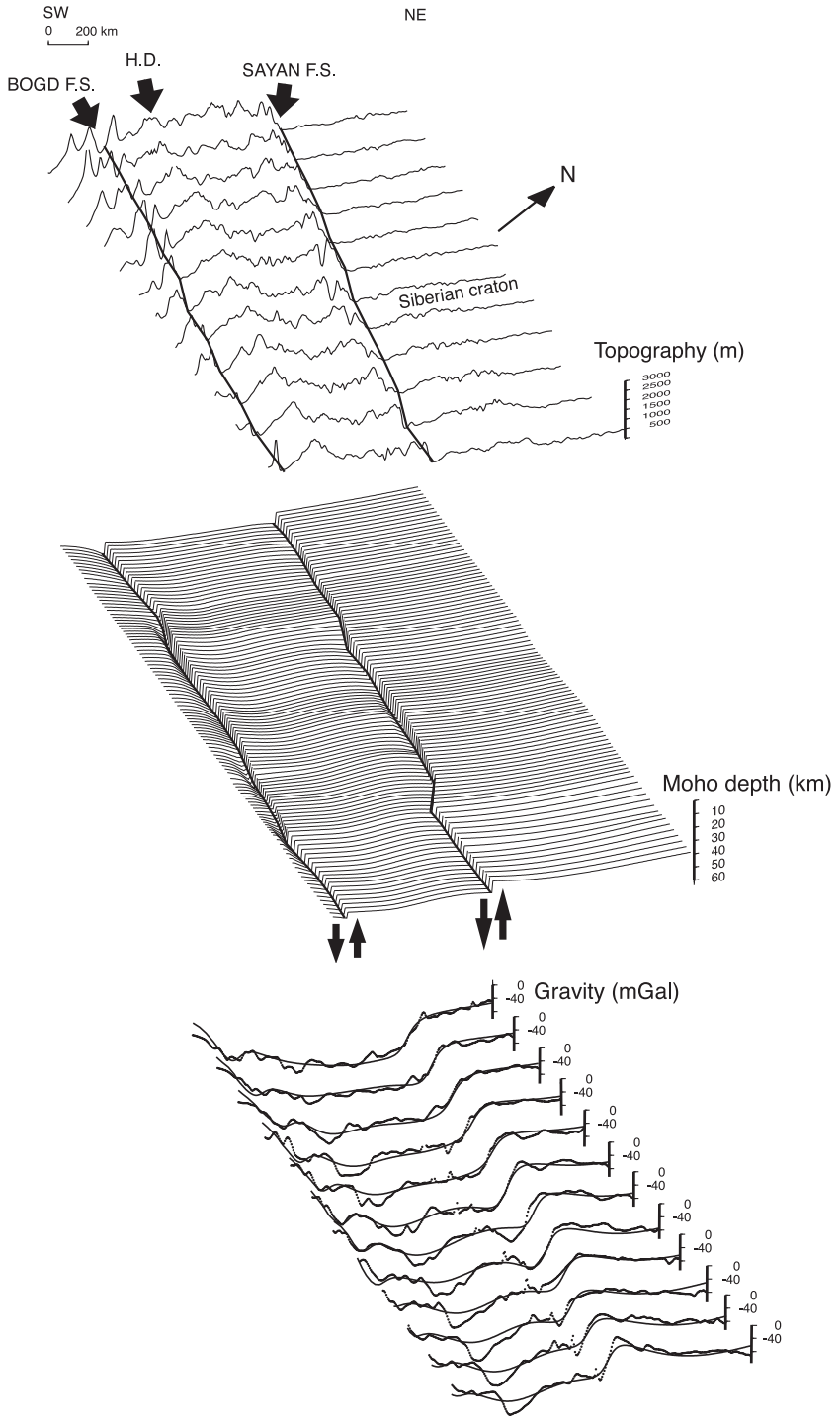

Fig. 5. (Top) Topography in meters along the 12 parallel profiles. Sayan and Bogd fault systems are indicated, as well as the Hangai dome (H.D., black arrows). (Center) Modeled Moho depth resulting from regional compensation of the topography and from flexure of the lithosphere close to the faults (arrows). (Bottom) Measured (thin line)/predicted (thick line) Bouguer gravity signal along the 12 parallel profiles. See Fig. 1b for location. N is for north.

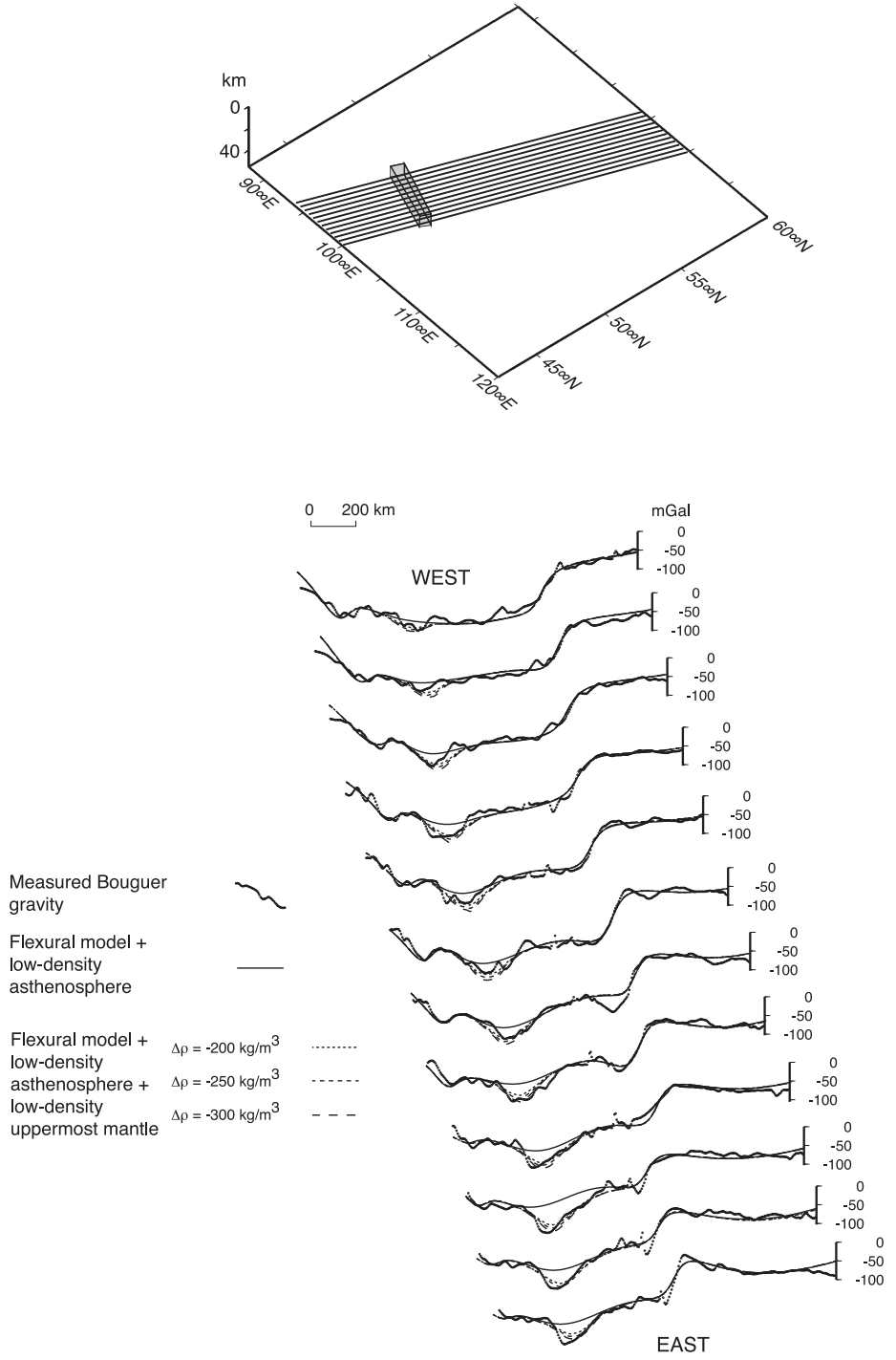

Fig. 6. (Top) Geometry of a low-density body (inset) located between 50 and 60 km depth, 10 km wide and 500 km long, with variable density reductions. The 12 parallel lines correspond to the profiles shown below. (Bottom) Twelve gravity profiles spaced from west (top) to east (bottom) across the Hangai–Hövsgöl region, showing the effect of the low-density uppermost mantle added to the flexural model (including the low-density asthenosphere). Spacing between lines is about 35 km. See Fig. 1b for location.

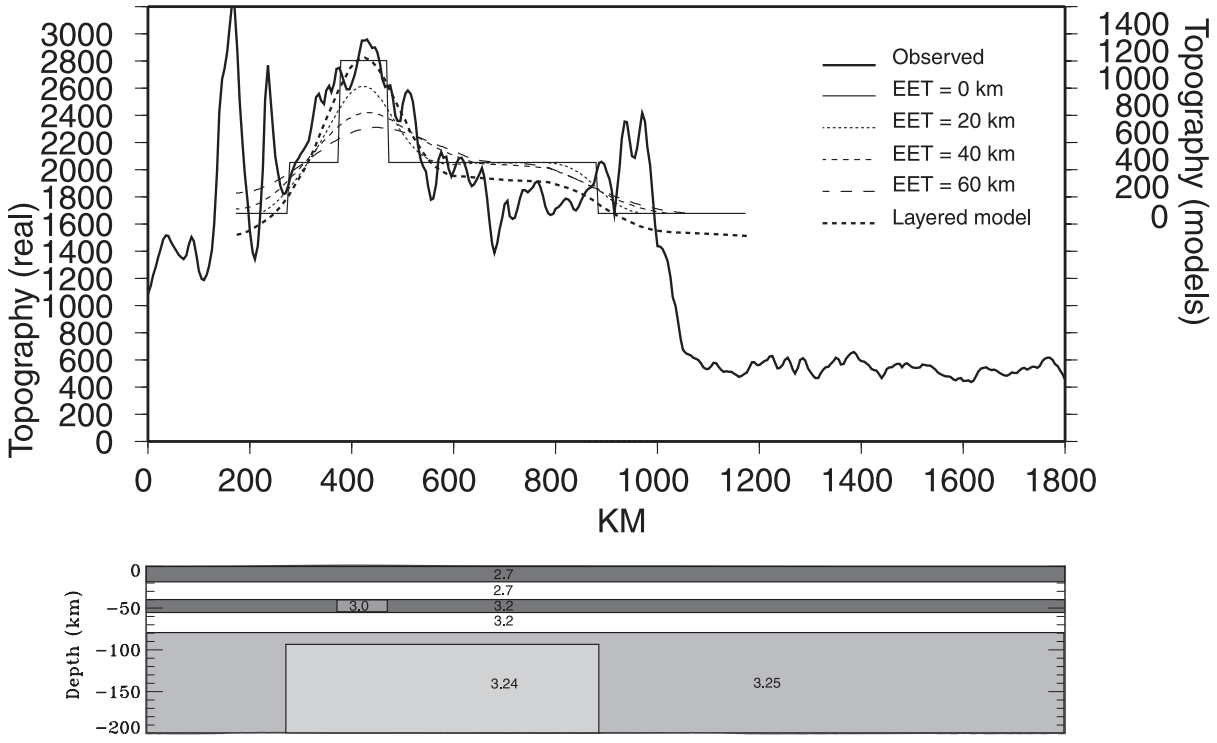

Fig. 7. (Top) Forward models of the isostatic uplift in response to the low-density bodies, compared to the observed topography. Left vertical scale corresponds to observed altitudes in meters; right vertical scale indicates modeled altitudes. EET models are elastic plate models with different EET values. Layered model comes from the computation with the PAROVOZ code [46], using a layered rheology as shown below. (Bottom) Initial configuration of the layered model, with density values. Dark gray areas correspond to elasto/brittle parts (upper crust and uppermost mantle); white areas correspond to elasto/ductile parts (lower crust and ductile upper mantle); light gray area is for asthenosphere.

non-uniqueness. However, these values compare reasonably well to other areas where magmatic underplating has been evidenced [45], and with estimates of velocity reduction due to heating of the uppermost mantle [46].

3.3. Forward modeling of the topography response

Now that the various contributions to the gravity field have been determined, we aim at quantifying the effect of mantle density anomalies on the present-day topography. We first compute the isostatic response of the lithosphere using a simple elastic plate model, with effective elastic thickness values ranging from 0 (Airy) to 60 km (Fig. 6). In any case, the modeled topography is shifted downwards by about 1600 m with respect to the actual one. This suggests that the first 1600 m of terrain elevation are not explained by density anomalies, but possibly by large-scale crustal thickening resulting from the Paleozoic and Mesozoic tectonomagmatic evolution [22]. This mean 1600-m-thick topography corresponds roughly to an $\sim$8-km-thick crustal root: if we refer to a zero-topography thickness of 40 km, this results in a mean 48-km-thick crust in central Mongolia, in good agreement with independent petrological constraints reported above. However, for elastic plate models, the fit to the observed topography is rather poor, which suggests that nonelastic deformation occurs. To check this point, we use the modeling code PAROVOZ (e.g., [47]). It is a hybrid finite element–finite differences fully explicit time-marching Lagrangian algorithm derived from the FLAC algorithm [48].

The model is two-dimensional and is made of

200×50 elements representing a 1000×200 km cross-section of the lithosphere and asthenosphere. The crust and mantle are both two-layered with an upper, brittle layer and a lower, non-Newtonian ductile layer (with the same rheological parameters as for flexural models). We introduce a 600×100 km low-density asthenosphere ($\Delta\rho = -10$ kg m^{-3}) and a 100×10 km low-density uppermost mantle ($\Delta\rho = -200$ kg m^{-3}). Horizontal motions of the left and right sides of the model are fixed, and hydrostatic pressure is applied at the bottom. The temperatures at the surface and at 150 km are 0°C and 1300°C, respectively. The maximum topography response is obtained after 100 ka, and does not significantly vary for greater time spans. Erosion is not included in the model, since we are interested only in the 'instantaneous' topographic response of the lithosphere. For the same reason, we do not investigate the effects of compressional velocities, due to lack of constraints on their time duration and to possible out-of-plane motions resulting from eastward escaping of the Mongolia area [14]. As shown in Fig. 7, the layered model provides a better fit than elastic plate models, advocating the use of a complex, layered continental rheology. We conclude that the asthenospheric density anomaly accounts for a mean elevation of about 400 m, whereas the anomalous uppermost mantle is responsible for an additional topography of about 700 m.

4. Discussion and conclusions

The gravity dataset analyzed here, together with independent information from mantle xenoliths and seismic tomography, allows us to propose a new interpretation of the crustal and lithospheric structure below the Hangai–Hövsgöl region, Mongolia, which – although not unique – is compatible with all relevant data. In addition to the mean large-scale elevation (~1600 m) of Mongolia probably coming (at least partly) from the pre-Cenozoic history, we determine there three distinct sources of gravity and topography anomalies: (1) local flexure of the lithosphere induced by present-day compressional tectonics, causing additional Moho deflection close to two major faults; (2) a deep-seated (100 km and more) anomalous, buoyant asthenosphere, causing a long-wavelength, low-amplitude, negative-gravity anomaly, a regional uplift of about 400 m and clear velocity reductions; and (3) low-density lowermost crust and/or uppermost mantle beneath the Hangai dome responsible for a high-amplitude gravity residual and a local uplift of about 700 m. We discuss hereafter the implications of these sources in terms of mechanical and geodynamical processes.

4.1. Flexural effects

The inferred state of lithospheric flexure near the Sayan and Bogd faults is consistent with the observed present-day tectonics. Indeed, the Gobi–Altai range (Fig. 1) is bounded by left-lateral strike-slip and reverse faults where vertical motions are likely to occur at a crustal level (e.g., [8,11]), and the Sayan fault (Fig. 1) lies on a major Paleozoic suture bounding the Siberian craton [16,22] which is characterized by recent tectonic activity ([16,42]) and a steep gradient at the Moho [36]. Across the Bogd and Sayan faults, the gravity signal is fitted by steps at the Moho of 5 and 10 km, respectively, in our modeling. These steps are partly due to a local, possibly inherited, compensation of the topography across these faults (see the Airy model in Fig. 3), but additional deflection of the Moho related to active transpression is needed to explain the amplitude of the gravity signal. High topography close to the faults is thus associated with downward flexure and deep crustal roots.

4.2. Deep-seated anomalous asthenosphere below Hangai–Hövsgöl

From our results, several questions arise concerning the processes responsible for the deep structures identified here: does the anomalous asthenosphere correspond to the top of a deep mantle upwelling, or is it a more surficial phenomenon, possibly due to variations of the lithospheric thickness? Alternatively, could density variations associated with partial melting provide the neces-

sary mantle buoyancy? Why are there almost no faults across the Hangai dome – indeed, the lithosphere should be thermally weakened and hence concentrate the deformation?

First, let us compare our results with previous interpretations of deep processes in this area. Our model disagrees with the qualitative one proposed by Windley and Allen [9] concerning the depth of the lithosphere–asthenosphere boundary beneath the Hangai–Hövsgöl dome. These authors, following Zorin et al. [18], suggest that the lithosphere is extremely thinned, but we have shown that a high-heat-flux mantle plume is unlikely, whereas a deep-seated (100 km or more) hot asthenosphere, combined with a low-density body at the Moho, is in quite good agreement with the gravity, tomography, volcanic and xenolith data. Cunningham [6,17] has proposed that asthenospheric flow creates a local extensional stress field that counteracts the regional NE compressional stress field, so that only scattered normal faulting can occur over the Hangai dome, and that the Baikal rift consequently locates in a 'crustal strain shadow'. From our analysis of the deep structure of the region, this is a possible explanation for the Hangai dome sensu stricto, considering that the gravitational potential energy coming from a lighter uppermost mantle favors extension as well. Concerning the origin of the deep anomaly, Cunningham [6] suggests that outward flow of the lithospheric mantle imposed by a crustal cratonic keel beneath Hangai causes inward flow of the asthenosphere and uplift of the dome. However, we note that the area of long-wavelength density and velocity anomalies widely exceeds the supposed extent of the Hangai Precambrian block (Fig. 2). Furthermore, this supposed 'cratonic keel' has nothing to compare with the gravity signature (high Bouguer gravity) and thermal structure (very low heat flow) of the Siberian craton ([30,36], Fig. 1). Therefore, it seems to us quite unlikely that a lithospheric mantle flow could be deflected there in response to an overthickening of the crust alone. Nor is a diversion of an asthenospheric mantle flow by a deep lithospheric root likely, given the inferred lithospheric thickness of $\sim$80 km.

What are the other possible sources for this anomalous buoyancy of the mantle occurring beneath Mongolia? Given the low amount of erupted lava, geochemical evidence for only slight heating (50–100°C) of the mantle, moderate surface heat flow, and the relatively large thickness of the lithosphere ($\sim$80 km), it is likely that partial melting cannot produce the required density reduction, but that this latter is simply due to heating of the asthenosphere below the solidus [5]. Mantle upwelling frequently occurs after collision of continental plates, due to thermal blanketing. Lowman and Jarvis [49] have shown that in the case of upper mantle convection, the place where upwelling occurs (with respect to the continental suture) depends on the width of the collided continental blocks. They have also proposed that upwelling can persist for a long time, causing tensional stresses not high enough to induce break-up of the overriding continental plate. We suggest that this is a possible explanation for the long-lived ($\sim$30–40 Ma), low-activity mantle upwelling occurring beneath Baikal and Mongolia, possibly in response to the collision of India and Eurasia [21].

4.3. Anomalous uppermost mantle beneath Hangai

Upwelling of hot asthenosphere in continental domains can lead to significant amounts of crustal underplating, depending on the source depth and temperature [45,50]. From the comparison of these results to the inferred thermal structure beneath Hangai ([26]; this study), we suggest that the deep-seated hot asthenosphere beneath Hangai–Hövsgöl can lead to a magmatic underplate thickness of maximally 10 km, and possibly less if the underplate is connected with the asthenospheric source via one or several low-density conduits. There is no clear evidence that the 'shallow' low-density body lies strictly in the mantle. However, several authors have identified intrusive and/or underplated bodies located beneath the Moho, as defined by the lowest-temperature lherzolite [25]: mafic granulites in the lower crust appear originated from underplated fractionated liquids and cumulates; Al-websterite cumulates are found at depths ranging between 50 and 60 km and garnet–pyroxenite cumulates occur beneath 60 km

[24]. Low-P velocity values ($\sim$7.8 km s^{-1}) in the uppermost mantle [19] beneath Baikal and Mongolia are also consistent with the presence of pyroxenite cumulates [44]. However, given the small density difference between pyroxenites and mantle peridotites ($\sim$40 kg m^{-3}), it is likely that underplating of such cumulates cannot account for the modeled 200 kg m^{-3} density reduction. Kopylova et al. [24] have evidenced from P–T analyses of crustal and mantle xenoliths that mafic granulites extend into the mantle (the crust–mantle transition being defined by the lowest-temperature lherzolite). Based on the work from Christensen and Mooney [44], it is clear that intrusion of mafic granulites in the uppermost mantle can account for part of the observed density/velocity reduction.

Acknowledgements

We thank D. Ionov for his explanations on xenolith analyses and E. Burov for providing his forward modeling code. Discussions with D. Cunningham and C. Ebinger were helpful. Detailed comments and suggestions from L. Lavier, A. Lowry, A. Caporali and an anonymous reviewer were appreciated. This research was funded by the CNRS-INSU Programme 'Intérieur de la Terre', the UPMC-IEC Cooperation Agreement, and the French Ministry of Foreign Affairs. This is UMR Geosciences Azur contribution no. 424. *[SK]*

References

[1] K. Stüwe, T. Barr, On the relationship between surface uplift and gravitational extension, Tectonics 19 (2000) 1056–1064.
[2] P.C. England, P. Molnar, Active deformation of Asia: From kinematics to dynamics, Science 278 (1997) 647–650.
[3] S. Cloetingh, E.B. Burov, A.N. Poliakov, Lithosphere folding: Primary response to compression? (from central Asia to Paris basin), Tectonics 18 (1999) 1064–1083.
[4] L. Fleitout, C. Froidevaux, Tectonics and topography for a lithosphere containing density heterogeneities, Tectonics 1 (1982) 21–57.
[5] A.R. Lowry, N.M. Ribe, R.B. Smith, Dynamic elevation of the Cordillera, western United States, J. Geophys. Res. 103 (2000) 23371–23390.
[6] W.D. Cunningham, Cenozoic normal faulting and regional doming in the southern Hangay region, central Mongolia: implications for the origin of the Baikal rift province, Tectonophysics 331 (2001) 389–411.
[7] W.D. Cunningham, B.F. Windley, D. Dorjnamjaa, J. Badamgarav, M. Saandar, A structural transect across the Mongolian Western Altai: Active transpressional mountain building in central Asia, Tectonics 15 (1996) 142–156.
[8] A. Bayasgalan, J. Jackson, J.F. Ritz, S. Carretier, Field examples of strike-slip fault termination in Mongolia and their tectonic significance, Tectonics 18 (1999) 394–411.
[9] B.F. Windley, M.B. Allen, Mongolian Plateau: Evidence for a late Cenozoic mantle plume under central Asia, Geology 21 (1993) 295–298.
[10] I. Baljinnyam, B.A. Borisov, A. Bayasgalan, A. Cisternas, M.G. Dem'yanovich, L. Ganbaatar, V.M. Kochetkov, R.A. Kurushin, P. Molnar, H. Philip, Y.Y. Vashchilov, Ruptures of major earthquakes and active deformation in Mongolia and its surroundings, Geol. Soc. Am. Mem. 181 (1993) 1–59.
[11] A. Bayasgalan, J. Jackson, J.F. Ritz, S. Carretier, 'Forebergs', flower structures, and the development of large intra-continental strike-slip faults: The Gurvan Bogd fault system in Mongolia, J. Struct. Geol. 21 (1999) 1285–1302.
[12] A.I. Kiselev, Volcanism of the Baikal rift zone, Tectonophysics 143 (1987) 235–244.
[13] K. Heki, S. Miyazaki, H. Takahashi, M. Kasahara, F. Kimata, S. Miura, N.F. Vasilenko, A. Ivashchenko, K.D. An, The Amurian Plate motion and current plate kinematics in eastern Asia, J. Geophys. Res. 104 (1999) 29147–29155.
[14] E. Calais, S. Amarjargal, New constraints on current deformation in Asia from continuous GPS measurements at Ulan Baatar, Mongolia, Geophys. Res. Lett. 27 (2000) 1527–1531.
[15] K.M. Larson, R. Bürgmann, R. Bilham, J.T. Freymueller, Kinematics of the India-Eurasia collision zone from GPS measurements, J. Geophys. Res. 104 (1999) 1077–1093.
[16] P. Tapponnier, P. Molnar, Active faulting and Cenozoic tectonics of the Tien Shan, Mongolia, and Baykal region, J. Geophys. Res. 84 (1979) 3425–3455.
[17] W.D. Cunningham, Lithospheric controls on late Cenozoic construction of the Mongolian Altai, Tectonics 17 (1998) 891–902.
[18] Y.A. Zorin, V.M. Kozhevnikov, M.R. Novoselova, E.K. Turutanov, Thickness of the lithosphere beneath the Baikal rift and adjacent regions, Tectonophysics 168 (1989) 327–337.
[19] A.I. Kiselev, A.M. Popov, Asthenospheric diapir beneath the Baikal rift petrological constraints, Tectonophysics 208 (1992) 287–295.
[20] S. Gao, P.M. Davis, H. Liu, P.D. Slack, Y.A. Zorin, N.A. Logatchev, M.G. Kogan, P.D. Burkholder, R.P. Meyer, Asymmetric upwarp of the asthenosphere beneath the

Baikal rift zone, Siberia, J. Geophys. Res. 99 (1994) 15319–15330.
[21] A. Yin, Mode of Cenozoic east-west extension in Tibet suggesting a common origin of rifts in Asia during the Indo-Asian collision, J. Geophys. Res. 105 (2000) 21745–21759.
[22] Y.A. Zorin, Geodynamics of the western part of the Mongolia-Okhotsk collisional belt, Trans-Baikal region (Russia) and Mongolia, Tectonophysics 306 (1999) 33–56.
[23] Geological map of Mongolian People's Republic, scale 1:3000000, in: N. Sodnom, A.L. Yanshin (Eds.), National Atlas of Mongolian People's Republic, Ulan-Baatar, 1990, 144 pp.
[24] M.G. Kopylova, S.Y. O'Reilly, Y.S. Genshaft, Thermal state of the lithosphere beneath central Mongolia: evidence from deep-seated xenoliths from the Shavarym-Saram volcanic center in the Tariat depression, Hangai, Mongolia, Lithos 36 (1995) 243–255.
[25] H.G. Stosch, D.A. Ionov, I.S. Puchtel, S.J.G. Galer, A. Sharpouri, Lower crustal xenoliths from Mongolia and their bearing on the nature of the deep crust beneath central Asia, Lithos 36 (1995) 227–242.
[26] D.A. Ionov, S.Y. O'Reilly, W.L. Griffin, A geotherm and lithospheric section for central Mongolia (Tariat region), in: M.F. Flower, S.L. Chung, C.H. Lo, T.Y. Lee (Eds.), Mantle Dynamics and Plate Interactions in East Asia, AGU Geodynamics Series 27, 1998, pp. 127–153.
[27] M.D. Khutorskoy, V.V. Yarmoluk, Heat flow, structure and evolution of the lithosphere of Mongolia, Tectonophysics 164 (1989) 315–322.
[28] A. Curtis, J. Trampert, R. Snieder, B. Dost, Eurasian fundamental mode surface wave phase velocities and their relationship with tectonic structures, J. Geophys. Res. 103 (1998) 26919–26947.
[29] M.H. Ritzwoller, A.L. Levshin, Eurasian surface wave tomography: group velocities, J. Geophys. Res. 103 (1998) 4839–4878.
[30] C. Petit, I. Koulakov, J. Déverchère, Velocity structure around the Baikal rift zone from teleseismic and local earthquake traveltimes and geodynamic implications, Tectonophysics 296 (1998) 125–144.
[31] A. Villaseñor, M.H. Ritzwoller, A.L. Levshin, M.P. Barmin, E.R. Engdahl, W. Spakman, J. Trampert, Shear velocity structure of central Eurasia from inversion of surface wave velocities, Phys. Earth Planet. Inter. 123 (2001) 169–184.
[32] S.V. Rasskazov, Magmatism related to the Eastern Siberia Rift System and the geodynamics, Bull. Centres Rech. Explor. Prod. Elf Aquitaine 18 (1994) 437–452.
[33] P. Wessel, W.H.F. Smith, New, improved version of Generic Mapping Tools released, EOS Trans. Am. Geophys. Union 79 (1998) 579.
[34] N.N. Puzyrev, M. Mandelbaum, S.V. Krylov, B.P. Mishenkin, G.V. Petrik, G.V. Krupskaya, Deep structure of the Baikal and other rift zones from seismic data, Tectonophysics 45 (1978) 15–22.
[35] E.B. Burov, F. Houdry, M. Diament, J. Déverchère, A broken plate beneath the North Baikal rift zone revealed by gravity modelling, Geophys. Res. Lett. 21 (1994) 129–132.
[36] C. Petit, E.B. Burov, J. Déverchère, On the structure and mechanical behavior of the extending lithosphere in the Baikal rift from gravity modeling, Earth Planet. Sci. Lett. 149 (1997) 29–42.
[37] G.D. Karner, A.B. Watts, Gravity anomalies and flexure of the lithosphere at mountain ranges, J. Geophys. Res. 88 (1983) 10449–10477.
[38] A. Caporali, Buckling of the lithosphere in western Himalaya: Constraints from gravity and topography data, J. Geophys. Res. 105 (2000) 3103–3113.
[39] F. Deschamps, R. Snieder, J. Trampert, Joint inversions of seismic and geodetic data in the uppermost mantle, Phys. Earth Planet. Inter. 124 (2001) 193–212.
[40] E.B. Burov, M. Diament, The effective elastic thickness (Te) of continental lithosphere: What does it really mean?, J. Geophys. Res. 100 (1995) 3905–3927.
[41] S.H. Kirby, A.K. Kronenberg, Rheology of the lithosphere: selected topics, Rev. Geophys. 25 (1987) 1219–1244.
[42] J. Déverchère, C. Petit, N. Gileva, N.A. Radziminovitch, V.I. Melnikova, V.A. San'kov, Depth distribution of earthquakes in the Baikal rift system and its implications for the rheology of the lithosphere, Geophys. J. Int. 146 (2001) 714–730.
[43] J.D. Byerlee, Friction of rocks, Pure Appl. Geophys. 116 (1978) 615–626.
[44] N.I. Christensen, W.D. Mooney, Seismic velocity structure and composition of the continental crust: A global view, J. Geophys. Res. 100 (1995) 9761–9788.
[45] R.S. White, D. McKenzie, Magmatism at rift zones: The generation of volcanic continental margins and flood basalts, J. Geophys. Res. 94 (1989) 7685–7729.
[46] S.V. Sobolev, H. Zeyen, M. Granet, U. Achauer, C. Bauer, F. Werling, R. Altherr, K. Fuchs, Upper mantle temperatures and lithosphere-asthenosphere system beneath the French Massif central constrained by seismic, gravity, petrologic and thermal observations, Tectonophysics 275 (1997) 143–164.
[47] A.N. Poliakov, Y. Podladchikov, C. Talbot, Initiation of salt diapirs with frictional overburden numerical experiments, Tectonophysics 228 (1993) 119–210.
[48] P.A. Cundall, Numerical experiments on localization in frictional materials, Ing. Arch. 59 (1989) 148–159.
[49] J.P. Lowman, G.T. Jarvis, Continental collisions in wide aspect ratio and high Rayleigh number two-dimensional mantle convection models, J. Geophys. Res. 101 (1996) 25485–25497.
[50] K.P. Furlong, D.M. Fountain, Continental underplating: Thermal considerations and seismic-petrologic consequences, J. Geophys. Res. 91 (1986) 8285–8294.